small NANO MICRO

Microfluidics

Screening Conditions for Rationally Engineered Electrodeposition of Nanostructures (SCREEN): Electrodeposition and Applications of Polypyrrole Nanofibers using Microfluidic Gradients

Hayden A. Burgoyne, Philseok Kim, Mathias Kolle, Alexander K. Epstein, and Joanna Aizenberg*

***A** rapid screening method for optimizing electrochemical deposition conditions of polypyrrole (PPy) nanostructures is reported. An electrochemical cell is integrated within a low-cost microfluidic system, in which electrochemical deposition is carried out across a linear concentration gradient of a reaction parameter. The protocol, refered to as the screening of conditions for rationally engineered electrodeposition of nanostructures (SCREEN), allows rapid screening of conditions for the production of specific morphologies by characterizing the electrodeposited samples produced within a chemical gradient. To demonstrate the utility of the SCREEN method, applications in tunable optical coatings and superhydrophobic surfaces are presented.*

1. Introduction

The growth of conductive polymers into various nanostructures has been of great interest in recent years due to the wide range of applications for which these polymers could be used. In particular, 1D nanofibers have been proposed as useful structures for electrochromic devices,[1–3] supercapacitors,[4,5] field-effect transistors,[6] controlled drug-release devices,[7] and chemical sensors.[8] Various approaches using both soft[9–11] and hard templates[12] have been used in the past to grow nanofibers, and simple, template-free approaches have been developed more recently.[13–16] The ability to control the formation of polypyrrole (PPy) nanofibers is of particular interest due to their high conductivity, environmental stability, and biocompatibility.[17] Furthermore, Py can be electrochemically polymerized,[18–20] allowing for much greater control over the location and duration of polymerization. However, the morphology, size, and density of electrodeposited PPy structures are acutely sensitive to the precise deposition conditions, such as concentration of monomer, concentration and pH of electrolytes, applied voltage, and time of deposition; even slight modifications of these conditions can lead to divergent morphologies (films, fibers, bowls, cones, etc.).[21–23] In order to find the optimized set of electrochemical deposition conditions for the growth of a desired particular morphology (e.g., nanofibers), multiple samples must be prepared from depositions in bulk solutions by varying a single parameter at a time for each experiment. Therefore these experiments typically require large volumes of reagents and substrates, become time-consuming, and generate a large volume of chemical waste.

Here we report a low-cost, benchtop-based, and *green* protocol that we refer to as SCREEN (screening conditions for rationally engineered electrodeposition of nanostructures), integrating a microfluidic gradient generator with an electrochemical cell to quickly screen a number of chemical

H. A. Burgoyne, Dr. P. Kim, Dr. M. Kolle, Dr. A. K. Epstein, Prof. J. Aizenberg
School of Engineering and Applied Sciences
Harvard University
Cambridge, MA 02138, USA
E-mail: philseok.kim@wyss.harvard.edu
Dr. P. Kim, Prof. J. Aizenberg
Wyss Institute for Biologically Inspired Engineering
Harvard University
Cambridge, MA 02138, USA
Prof. J. Aizenberg
Department of Chemistry and Chemical Biology
Harvard University
Cambridge, MA 02138, USA

DOI: 10.1002/smll.201200888

parameters that govern the morphology of the resultant electrodeposited PPy on a substrate. The use of microfluidic gradients to perform experiments with a range of parameters has been previously demonstrated with applications such as biological and chemical sensors as well as fabrication of nanostructured materials.[24–26] The method does not require costly and time-consuming photolithographic processes to fabricate the microfluidic devices; instead it uses inexpensive materials and rapid fabrication techniques such as Kapton tape and laser cutting. Using the SCREEN procedure, we are able to create various electrodeposition conditions that lead to numerous nanoscale morphologies of electrodeposited PPy, each of which is potentially suitable for various applications. The information gathered from the gradient experiments is verified in bulk deposition in a conventional electrochemical cell over a large area. Given the broad range of their potential applications, PPy nanofibers are investigated in more detail, and we demonstrate quickly optimized deposition conditions that result in fibrous surfaces with controlled optical and wetting characteristics. We envision that our method can serve as a toolkit for optimizing the electrochemical deposition processes for many other materials, such as minerals, inorganics, hydrogels, or hybrid materials. SCREEN will enable better understanding of the nucleation and growth behavior and facilitate solution-based directed electrochemical synthesis and assembly of novel nanomaterials.

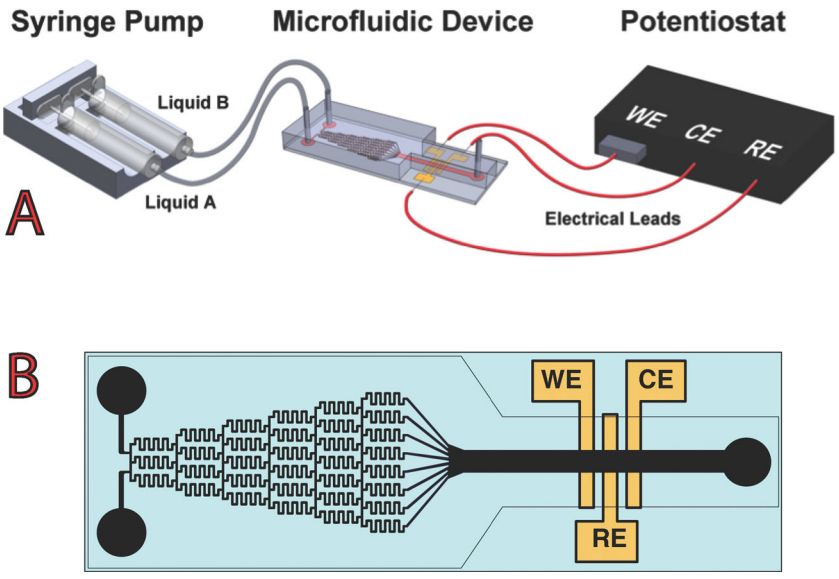

Figure 1. A) Schematic of experimental setup. The microfluidic device creates a gradient of two input liquids. A potential is applied via a potentiostat to the electrodes (WE: working electrode; CE: counter electrode; RE: reference electrode) embedded within the microfluidic device, where electrochemical polymerization occurs across the chemical gradient. B) CAD image of overhead view of the microfluidic channels and electrodes on a glass microscope slide.

2. Results and Discussion

2.1. Screening of Deposition Conditions

A schematic of the experimental setup is shown in **Figure 1**. The microfluidic device creates a concentration gradient of the two input liquids through a series of branching, recombining, and mixing channels under laminar flow until a gradient with a suitable number of intermediate concentrations is reached. The gradient is then merged into a single channel, which guides the graded reagent solution over the electrodes where the electrodeposition is induced. The device is fabricated by first using a commercial laser cutter to create the gradient generator pattern in Kapton tape attached to a glass slide. Polydimethylsiloxane (PDMS) is cast on this master pattern to prepare a microfluidic gradient generator, which is then bonded to a glass slide with patterned electrodes for electrodeposition. A potential is applied via a potentiostat to the three electrodes in the microfluidic channel, and following electrochemical polymerization across the chemical gradient, the resultant continuum of morphologies is observed. The concentration profile is confirmed to be linear by measuring the fluorescence intensity gradient of Rhodamine dye under UV light, as previously described.[27] Furthermore, the electrodes are made to be thin relative to the length of the channel so that the gradient can be utilized before diffusion smoothes the gradient profile and so that the concentration of reactants consumed during electrodeposition does not significantly change over the width of the electrode. Therefore, an ideal linear concentration gradient, constant across the entire width of the electrode, is assumed when caluculating concentration corresponding to a specific location in the gradient.

The deposition conditions for growing 1D polypyrrole nanofibers without using a template have been previously investigated,[13,14] but our method provides fast access to a large range of parameters and high resolution in the parameter space, enabling rapid discovery of ideal deposition conditions. Using previously identified conditions as a baseline about which the gradients could be set, the following chemical parameters are explored: the concentration of the pyrrole (Py) monomer, the concentration of the phosphate buffered saline (PBS), and the pH of the PBS. After deposition, the morphologies arising from a large set of electrochemical parameters are observed, and the conditions for most consistently growing 1D PPy nanofibers can be determined.

2.1.1. Screening for the Optimal Monomer Concentration

A concentration gradient of Py monomer from 0 to 0.15 M in 0.25 M PBS (pH 6.8) and 0.07 M lithium perchlorate ($LiClO_4$) was established across the electrodeposition zone. A potential of 0.85 V versus the gold pseudo-reference electrode was constantly applied for 10 min. The scanning electron microscopy

small 2012,
DOI: 10.1002/smll.201200888

NANO MICRO small

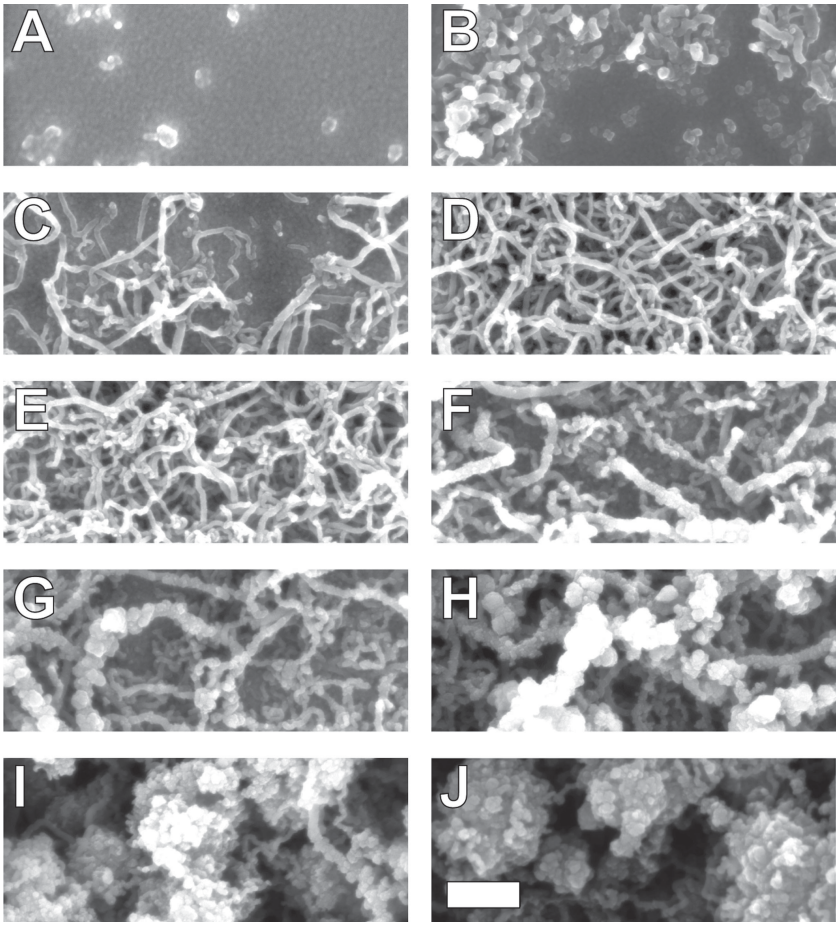

Figure 2. SEM images of different regions of a single sample grown under a gradient of Py concentration with concentrations of A) 0.014, B) 0.027, C) 0.041, D) 0.055, E) 0.068, F) 0.082, G) 0.095, H) 0.109, I) 0.123, and J) 0.136 M with 0.07 M $LiClO_4$ and 0.25 M PBS (pH 7.5). The scale bar for all images is 800 nm. Images were taken at evenly spaced intervals along the direction of the gradient.

(SEM) images of the morphologies formed on the working electrode after electrodeposition are shown in **Figure 2**. With very low Py concentration, the growth was predictably sparse with random nucleation of small amounts. As the concentration rose, both the rate of nucleation and growth increased, showing more deposition and the beginning of a preference for one-dimensionality of the growing polymer. With continually increasing Py concentration, the rate of new nucleation (parasitic nucleation) began to overwhelm the growth rate of unbranched, 1D fibers and resulted in cauliflower-like structures. The most consistent growth of long, thin nanofibers was observed near the center of the gradient, corresponding to a concentration of 0.075 M Py. This concentration was used for many subsequent experiments to further optimize other parameters.

2.1.2. Screening for the Optimal pH Range

A gradient of the pH of 0.25 M PBS was established between 5 and 8 while the concentrations for Py and $LiClO_4$ were kept constant at 0.075 and 0.07 M, respectively. A potential of 0.85 V was constantly applied for 10 min. In **Figure 3**, the pH had a major effect on the observed morphologies, as the rate of polymerization tends to be higher at lower pH. At a slightly basic pH, fibrous morphology was consistently observed. At lower pH, thicker films of PPy covered the surface with hierarchical structures of 10–100 μm mounds covered with much smaller 100 nm bumps. The deposition condition we found for this two-tiered hierarchical structure is remarkably useful because it can be created via a single-step deposition. Furthermore, by performing a two-step deposition process in which a second layer is deposited on top of this hierarchical surface using the conditions that yield nanofibers, the surface can be made to display three-tiered hierarchy. The functions of such a multiscale surface topography include extreme wettability properties, i.e., superhydrophillicity or superhydrophobicity, depending on surface treatment after deposition.[28] Furthermore, at the lowest pH, conical structures begin to form, reminiscent of conductive polymer structures used for supercapacitors.[29]

2.1.3. Screening for the Optimal PBS Concentration

A concentration gradient of PBS was established in a microfluidic device from 0.15 to 0.35 M (pH 7.5) while the concentrations for Py and $LiClO_4$ were kept constant at 0.075 and 0.07 M, respectively. A potential of 0.85 V was constantly applied for 10 min. The effect of the concentration of PBS in this range was found to be minimal. PPy deposition was observed over the entire sample, and changes in morphology were very slight and randomly distributed, as shown in the Supporting Information (SI), Figure S1. Over multiple samples, the area corresponding to 0.25 M PBS was observed to have relatively consistent morphology and was fully covered with electrodeposited PPy.

Each of these results was verified to be reproducible. Furthermore, given the results of the pH gradient, which showed that more consistent nanofibers could be achieved at a higher pH, the experiment investigating the gradient of the monomer concentration was repeated at different pH values as well (5.8, 6.8, and 7.5).

Our SCREEN technique of using a microfluidic gradient generator to combinatorially determine deposition conditions proved to be extremely efficient, in both time and cost, compared to testing individual conditions in bulk solution on a large sample. A single experiment provided information with enough resolution to find the ideal conditions for deposition of a desired morphology from a continuum of values of a chemical parameter being investigated. The bulk deposition process requires significantly more consumed materials,

DOI: 10.1002/smll.201200888

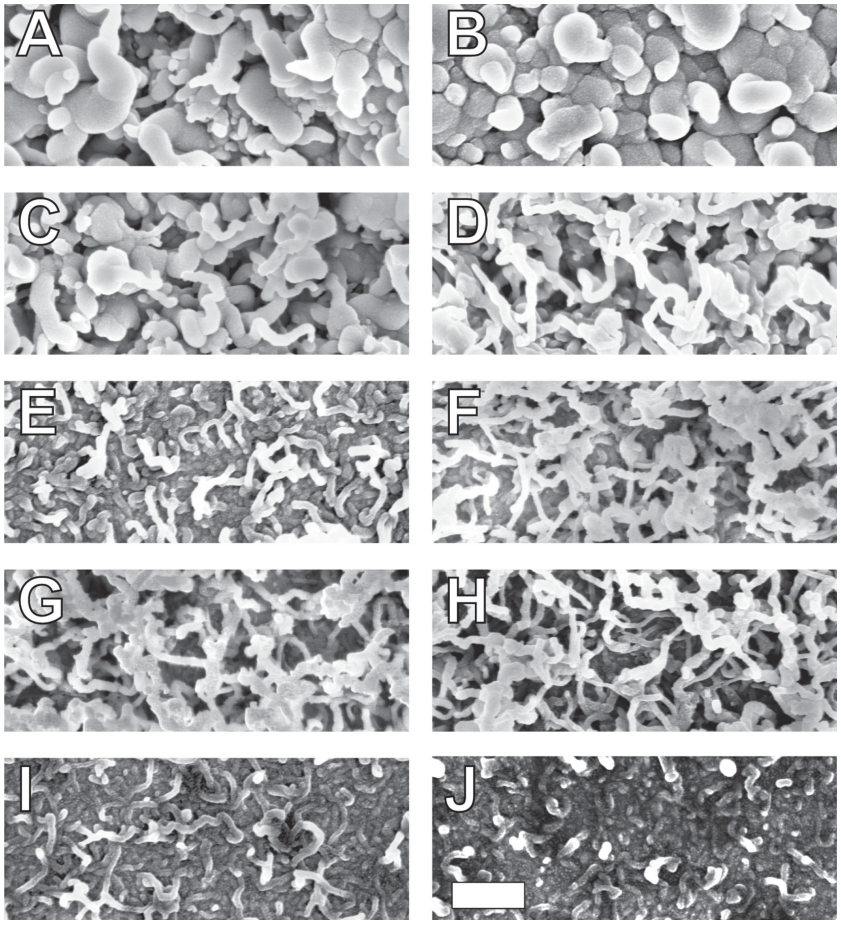

Figure 3. SEM images of different regions of a single sample grown with 0.075 M Py, 0.07 M $LiClO_4$, and 0.25 M PBS under a pH gradient approximately corresponding to pH A) 5.6, B) 5.9, C) 6.2, D) 6.5, E) 6.8, F) 7.1, G) 7.4, H) 7.7, I) 8.0, and J) 8.3. The magnification is the same in all images; scale bar is 800 nm. Images were taken at evenly spaced intervals along the direction of the gradient.

produces more chemical waste, and only yields a single data point. The entire SCREEN protocol for producing a sample grown with our gradient device requires about 5 h including fabrication of the device and electrodeposition, whereas a single sample grown in bulk requires about 2 h. Therefore, when multiple data points are necessary, it is highly efficient to use this microfluidic device and the SCREEN method. Additionally, the cost per sample created is very comparable to those deposited in bulk; therefore it is also cost-effective to use the microfluidic device when multiple data points are desired.

2.2. Testing Select Structures for Potential Applications

The ability to control the morphology, size, and hierarchy of nanostructures that decorate the surface has been recently introduced as a powerful tool to tune various physical and chemical surface properties, such as catalytic activity, wetting and adhesive characteristics, and optical properties.[12,20,30] By using the SCREEN approach we can extract experimental conditions that lead to specific morphologies of interest and then use these parameters to produce a large-area, uniform coating and test its properties. To fabricate large-area samples, a silicon wafer coated with gold in the same manner as the electrodes in the SCREEN device was used as the working electrode. A platinum mesh was used as the counter electrode and a Ag/AgCl (saturated with NaCl) electrode served as the reference electrode. A linear scan of voltage versus current showed that 0.85 V would yield nearly the same current density as with the microfluidic electrochemical setup, suggesting similar rates of deposition. The large-scale samples were imaged using field-emission scanning electron microscopy (FE-SEM), confirming that the large-area deposition using the conditions determined by SCREEN led to morphologies identical to those identified by microfluidic screening. Two exemplary morphologies—fibrous network and cauliflower surfaces—are shown in **Figure 4**.

While a range of applications can be envisioned for the uniform surfaces decorated with these morphologies, we present here their use in two potential areas: controlling optical properties and surface wetting characteristics.

2.2.1. Towards Applications in Optics and Photovoltaics

PPy has been reported to serve as an efficient hole transporter in dye-sensitized solar cells.[31] In addition, the growth of

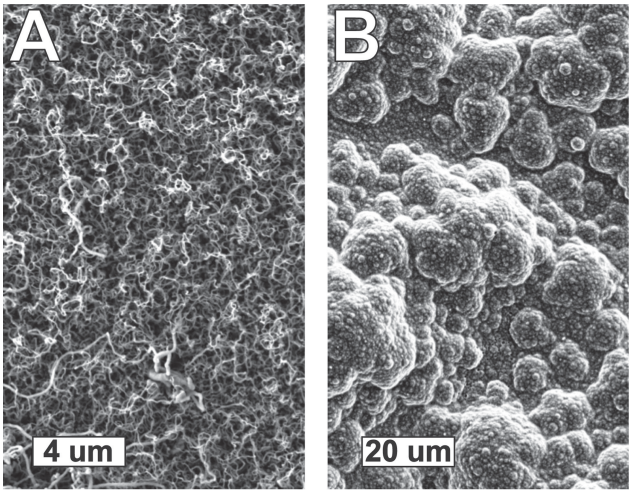

Figure 4. FE-SEM images of the morphologies resulting from bulk deposition using the conditions optimized by SCREEN method. The sample in (A) was deposited with 0.075 M Py, 0.25 M PBS (pH 7.5), and 0.07 M $LiClO_4$ at 0.85 V for 10 min. The sample in (B) resulted from bulk deposition at low pH with 0.075 M Py, 0.25 M PBS (pH 5.8), and 0.07 M $LiClO_4$ at 0.85 V for 10 min.

small 2012,
DOI: 10.1002/smll.201200888

NANO MICRO small

hierarchical PPy structures with high surface area and large scattering and absorption cross-section could be beneficial for the development of ultra-black surface coatings similar in function to the melanin-loaded structures found on the wing scales of *Papilio* butterflies.[32] This could be beneficial for efficient thermal collectors or provision of visual stark contrast in a variety of active and passive display technologies. Since PPy exhibits a broad band absorption in the visible range, the reflection of the films was characterized across the gradients in order to observe how the reflectance varied with the morphology. The intensity of white light reflected from the PPy on the gold electrode was measured using a micro-spectroscope allowing collection of spectra from 20 μm wide spots on the sample. After 10 min of deposition, a sample grown under a gradient of Py monomer showed a dramatic change from the reflection of bare gold at low concentrations of Py to effectively zero reflectance once a film had been deposited. These measurements are shown in **Figure 5**A. The reflectance of PPy samples across pH and PBS concentration gradients was also measured and is shown in Figure 5B and C, respectively. In electrochromic applications of conductive polymers, such as windows or displays, the optical properties such as reflectance and transmittance are critical. Our SCREEN method could therefore be used to screen conditions to predict those that produce the desired absorption and transmittance.

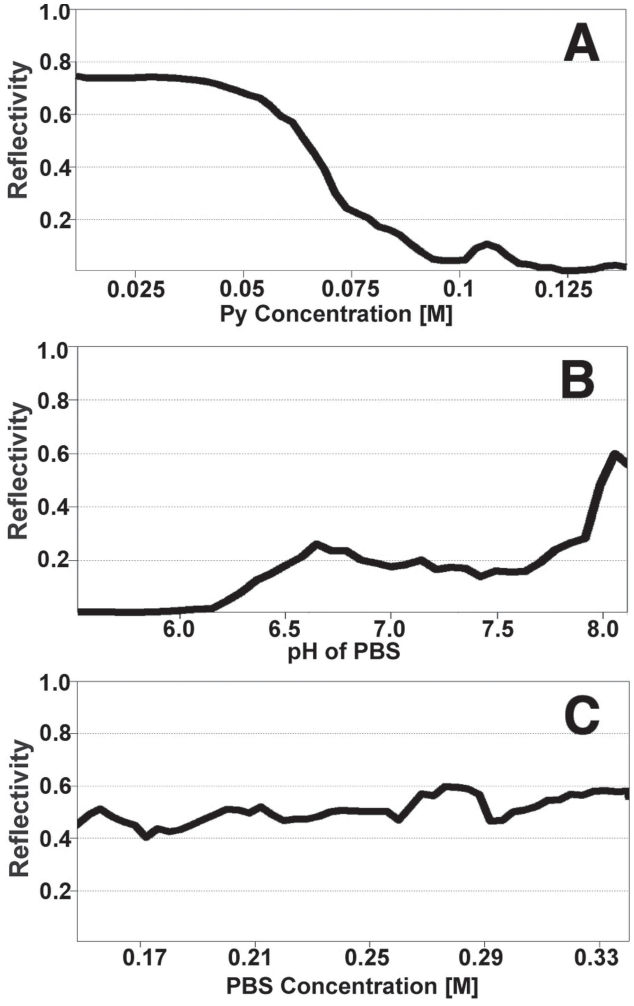

Figure 5. Plots of the reflectivity of different samples with PPy structures on the gold electrode after 10 min of deposition along each of three gradients. Each data point represents the reflectivity of a spot of 20 μm diameter acquired by scanning along the sample in the direction of the gradient under which the sample was deposited. Sample (A) was deposited with a Py concentration gradient, (B) was deposited with a pH gradient, and (C) was deposited with a gradient of PBS concentration.

2.2.2. Tunable Wetting Properties

In many situations, it is necessary to control the wetting properties of a surface, that is, how a liquid either spreads on the surface or beads up and even rolls off. Anti-fog shower mirrors must be hydrophilic such that moisture condenses in a specular film that maintains the optical function of the mirror. Vehicle windshields, in contrast, are chemically treated for water repellency to promote water removal by wind. But to achieve both greater control of wetting and wetting function longevity, more than surface chemical treatments must be used. The physical texture of a surface, specifically the roughness and presence of tall or overhanging structures, generally leads to an amplification of the surface chemistry, with the result in principle ranging from full wetting (0° apparent contact angle between liquid and solid) to full repellency (180°).[33–35] The natural model of the lotus leaf, which combines micro- and nanoscale surface structures with hydrophobic wax chemistry, has motivated two decades of work in designing synthetic surface morphologies to control wetting.[36–38]

PPy nanofiber arrays have recently been shown to exhibit superhydrophilicity with a contact angle near zero,[13,20] but the same fiber network can also exhibit superhydrophobicity[39,40] after appropriate chemical treatment. Therefore, large-area samples of some PPy morphologies were tested for contact angle first with water in air and then with mixtures of ethanol and water in air. Furthermore, the wetting properties of a hierarchical structure created through a multiple-step, multiple-material process by depositing PPy nanofibers onto an array of high-aspect-ratio epoxy posts were also tested to observe wetting characteristics of liquids with different surface tensions.

Large-area samples of both nanofibers (Figure 4A) and low-pH, cauliflower morphologies (Figure 4B) were treated with *1H,1H,2H,2H*-perfluorooctyl trichlorosilane for 24 h in a vacuum desiccator. Therefore, with identical surface chemistry, the effects of the different nanostructures on wetting angle could be determined. The average contact angle of water droplets placed on the PPy nanofiber-coated surface (**Figure 6**A) in normal atmosphere was measured to be 148° with a standard deviation of 9°. The water contact angle of the single-deposition, PPy cauliflower structure (Figure 6B) created via the single deposition at low pH was 127° with a standard deviation of 10°. The difference of the water contact angles on these surfaces is attributed to the much higher surface roughness, reentrant curvatures, and trapped air of the PPy nanofiber network than the single-deposition hierarchical structure.

The natural "lotus effect" of liquid repellency of a surface by roll-off is limited to water. However, water possesses

DOI: 10.1002/smll.201200888

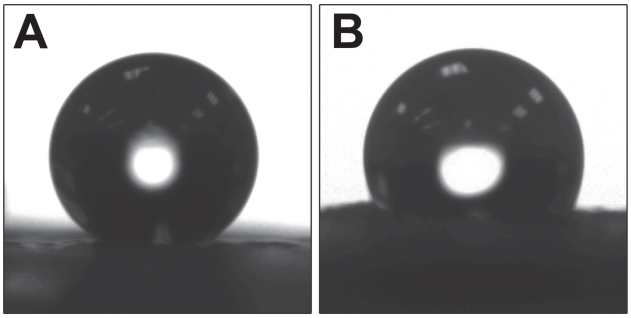

Figure 6. Photographs of a water droplet placed on large-area samples of bulk deposited nanostructured PPy to compare the contact angles of the two surfaces. Deposition conditions in (A) were 0.075 M Py, 0.25 M PBS (pH 7.5), 0.07 M $LiClO_4$, 10 min at 0.85 V, resulting in nanofibers. Deposition conditions in (B) were 0.075 M Py, 0.25 M PBS (pH 5.8), and 0.07 M $LiClO_4$, 10 min at 0.85 V, resulting in hierarchical structures.

exceptionally high surface tension, 72.7 mN m^{-1} at 25 °C, in contrast to many liquids relevant in engineering settings. For instance, the surface tension of alcohols is 22.1 mN m^{-1} at 25 °C, causing even dilute mixtures of ethanol and water to wet extremely readily on most surfaces. A recent study reported that a bacterial biofilm, unlike the lotus, could resist wetting by such low surface tension mixtures owing to both surface chemistry, reentrant multiscale topography, and possibly other factors.[41] Adapting the same methodology, we characterized the wetting properties of surfaces with PPy nanofibers (**Figure 7**A–C) as a function of surface tension by varying the test liquid's volume fraction of ethanol. In addition to starting with a flat Au-coated epoxy substrate, we also employed a Au-coated high-aspect-ratio (AR = 32) epoxy nanopost array called nanograss (NG) as described previously,[42,43] and we decorated select flat and nanopost substrates with PPy fiber. The surfaces thus represented conditions of no topography, a single-length-scale structured surface, and a hierarchical surface. All were chemically treated to be hydrophobic, as described above.

As shown in Figure 7d, as the ethanol volume fraction of the test liquid was increased (and the surface tension thus decreased) the contact angle of liquid on the flat surface decreased from ~110° to ~40°, whereas both structured surfaces exhibited superhydrophobicity (>150°) up to 40% ethanol. As the surface tension was further decreased, the nanoposts failed to exhibit superhydrophobicity, undergoing a Cassie (liquid atop the structures) to Wenzel (fully wetted) transition. The nanofiber-decorated flat surface failed more gradually between the 50% and 70% ethanol levels, and the hierarchical nanofiber surface robustly maintained a Cassie state up to 80% ethanol before gradually failing above 80% ethanol. The superhydrophobic robustness of the hierarchical surface against up to 80% ethanol, and in a separate experiment, against the repeated impact of terminal-velocity water drops normal to the surface, is consistent with the greatly increased interfacial area created between the test liquid and air trapped within the posts and reentrant PPy fibrous network.

Because of the high surface area, porosity, and three-dimensionality of the electrodes coated in PPy nanofibers, these surfaces would also be useful for either impregnation with another material or a secondary deposition of a non-conductive material. For example, the nanofiber network would be a suitable substrate for the addition of a lubricating film to create a slippery surface using the SLIPS (slippery liquid infused porous surfaces) method.[44] Furthermore, our nanofiber networks could provide a 3D electrode onto which hydrogel could be electrochemically deposited.[45] The possible thickness of electrochemically deposited hydrogel is limited by the poor conductivity of the hydrogel. However, starting with a 3D substrate could provide the conductive pathways for the electrochemical deposition of thicker films of hydrogel.

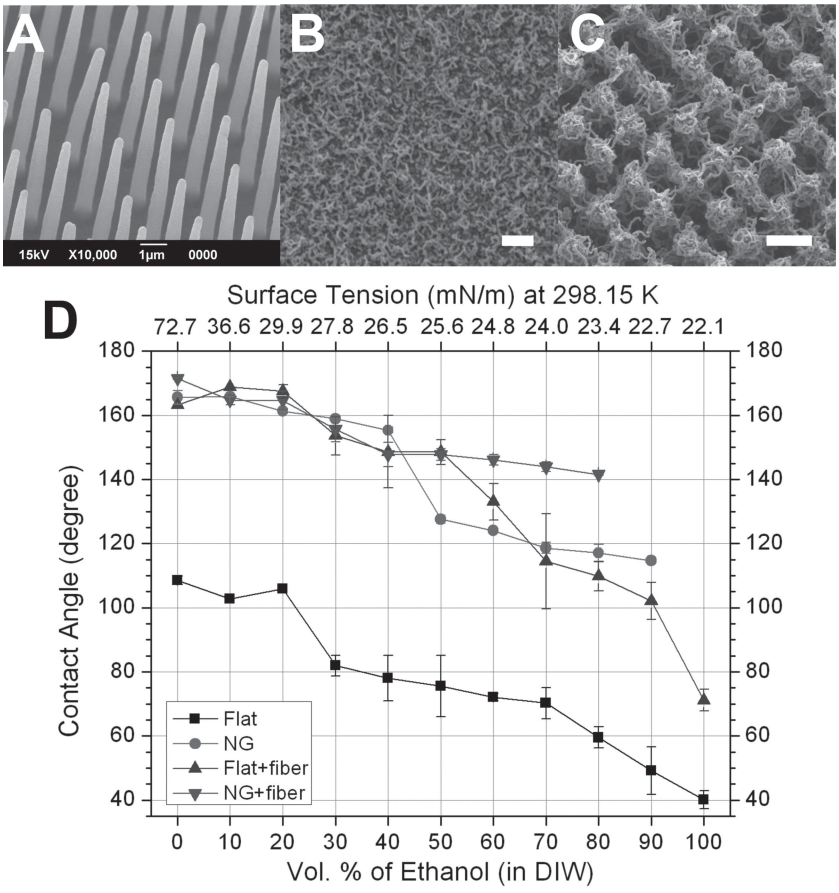

Figure 7. Three nanostructured surfaces and their wetting properties. SEM images of A) square array of height = 8 μm, diameter = 200 nm epoxy nanopillars with 2 μm pitch, B) PPy nanofiber decorating a flat substrate, C) a hierarchical structured surface combining (A) and (B). Scale bars represent 2 μm. D) Static contact angles of a droplet of water–ethanol mixture on these substrates. Flat: flat epoxy substrate; NG, Flat + fiber, and NG + fiber represent the structures shown in (A), (B), and (C), respectively.

small 2012,
DOI: 10.1002/smll.201200888

3. Conclusion

The novel screening device reported here, created by integrating the microfluidic gradient generator with an electrochemical cell for deposition of materials, provides a powerful method for rapid discovery of ideal conditions for the electrodeposition of arbitrary structure morphologies. We have shown that our method can be used to optimize parameters to find materials suitable for many desired applications.

Using SCREEN, the parameters that control the deposited morphologies of PPy are efficiently mapped with a small number of low-cost and rapid experiments. Our benchtop microfluidic-electrodeposition device, requiring no cleanroom tools for fabrication, robustly establishes linear chemical gradients for continuous screening of electrodeposition conditions. By varying the concentration of Py monomer, concentration of PBS, and the pH of PBS, our method has rationally produced ideal conditions for building functional hierarchical nanostructures that demonstrate extreme optical absorption and wettability properties, as just two examples of the application potential of PPy with precisely controlled nanoscale morphology. Given its cost and time efficiency, we believe that SCREEN will be a powerful tool for fabricating future functional materials by electrochemical deposition reactions.

4. Experimental Section

Device Fabrication: Shadow masks were designed using a CAD program and were fabricated by TechEtch. Electrodes were fabricated through thermal evaporation (Cressington 308) with a shadow mask onto a 1 inch × 3 inch glass microscope slide. Working, counter, and pseudo-reference electrodes were all approximately 200 nm thick Au with 20 nm thick Ti as an adhesion layer.

Microfluidic channels were fabricated via a multi-step replication process. First the outline of the channels was laser cut using a VersaLaser into a layer of 2 Mil Kapton tape adhered to a 1 inch × 3 inch glass slide. The excess Kapton was removed leaving only the embossed master. The master was treated with *1H,1H,2H,2H*-perfluorooctyl trichlorosilane (Gelest) for 24 h in a vacuum desiccator. PDMS (Dow Sylgard 184, 10:1 base to hardener ratio) was cast on the Kapton master at 70 °C for 4 h. The PDMS with embedded channels was then either oxygen plasma treated for 10 s and directly bonded onto a glass slide with deposited electrodes, or used to create a new UV-curable epoxy (UVO-114, Epotek) master for further replication. A biopsy punch was used to create the inlet and the outlet holes in the PDMS and 1 mm outer diameter surgical tubing was inserted into the holes. Because the PDMS was permanently bonded to the glass slide with electrodes, it was necessary to destroy the device to retrieve the sample for imaging studies. Therefore a new microfluidic device had to be fabricated for each sample, with the entire process requiring about 2 h once the master pattern was fabricated.

Microfluidic Gradient Generator Design: The design of the microfluidic gradient generator was inspired by previous studies.[27] The gradient is created by a series of branching, recombining and mixing steps which creates 8 distinct steps in the concentration of the chemical parameter between the two input concentrations. These steps are then recombined into a single large channel. Through the same diffusion process that mixed each recombination in the 200 μm mixing channels, the stepped gradient is smoothed into a pseudo-continuous linear gradient as it passes over the electrodes.

Electrodeposition: All chemicals were purchased from Sigma-Aldrich and used as received except for pyrrole. Pyrrole was purified by double filtering through an alumin-packed plastic disposable syringe immediately before use, as described previously.[43]

The flow rate through the microfluidic channels was maintained at 10 μL min^{-1} by a syringe pump (PhD Ultra, Harvard Apparatus). Sufficient time was allowed for bubbles to exit the system and for a stable gradient to be established. The potential was applied by a computer-controlled potentiostat (Versastat 3, Princeton Applied Research).

SEM Images: SEM images were obtained using either a Zeiss FE-SEM Supra 55VP or a Zeiss FE-SEM Ultra55 with an in-lens detector at an acceleration voltage of 3 kV.

Spectroscopic Characterization: Using a Leica DMRX Microscope, light reflected from the spots of 20 μm diameter on the sample was coupled into a fiber and guided into a USB 200 spectroscope (Ocean Optics). The intensity of reflected light was measured in a grid of 1000 individual 20 μm spots along the length and the width of the samples. The intensity was averaged across the visible spectrum and across the width of the sample to estimate the reflectivity of the material along the dimension in which the gradients were formed.

Contact Angle Experiments: Water contact angle experiments were performed by first creating large sample areas using bulk deposition in the conditions found from the gradient experiments. The samples were treated with *1H,1H,2H,2H*-perfluorooctyl trichlorosilane (Gelest) for 24 h in a vacuum desiccator. Small droplets of water were placed in multiple areas over the surface of the samples and observed using a video camera. The angle was then estimated from the photos using photo analysis software (CAM KSV 100).

Supporting Information

Supporting Information is available from the Wiley Online Library or from the author.

Acknowledgements

This work was partially supported by the U.S. Department of Energy, Office of Basic Energy Sciences, and the Division of Materials Science and Engineering, under award number DE-SC0005247 (hierarchical nanostructure fabrication on high-aspect-ratio structures and 3D electrodes for hydrogel deposition), and the U.S. Air Force Office of Scientific Research Multidisciplinary University Research Initiative under award number FA9550-09-1-0669-DOD35CAP (optical properties). Part of this work was also performed at the Center for Nanoscale Systems (CNS) at Harvard University, a member of the National Nanotechnology Infrastructure Network (NNIN), which is

DOI: 10.1002/smll.201200888

supported by the National Science Foundation under NSF award no. ECS-0335765. We thank Prof. Robert Wood and Prof. George Whitesides for the use of equipment and Mr. Wilmer Adorno for technical assistance, and Dr. Michael Aizenberg for comments on the manuscript.

[1] Q. Pei, G. Zuccarello, M. Ahlskog, O. Inganas, *Polymer* **1994**, *35*, 1347–1351.
[2] W. Lu, A. G. Fadeev, B. Qi, E. Smela, B. R. Mattes, J. Ding, G. M. Spinks, J. Mazurkiewicz, D. Zhou, G. G. Wallace, D. R. MacFarlane, S. A. Forsyth, M. Forsyth, *Science* **2002**, *297*, 983–987.
[3] L. Hu, G. Gruner, D. Li, R. B. Kaner, J. Cech, *J. Appl. Phys.* **2007**, *101*, 016102.
[4] R. Liu, S. I. Cho, S. B. Lee, *Nanotechnology* **2008**, *19*, 215710.
[5] J. Huang, K. Wang, Z. Wei, *J. Mater. Chem.* **2010**, *20*, 1117–1121.
[6] J. A. Merlo, C. D. Frisbie, *J. Phys. Chem. B* **2004**, *108*, 19169–19179.
[7] M. R. Abidian, D. H. Kim, D. C. Martin, *Adv. Mater.* **2006**, *18*, 405–409.
[8] Q. Ameer, S. B. Adeloju, *Sens. Actuators B* **2005**, *106*, 541–552.
[9] W. Shi, P. Liang, D. Ge, J. Wang, Q. Zhang, *Chem. Commun.* **2007**, 2414–2416.
[10] J. Huang, I. Ichinose, T. Kunitake, *Chem. Commun.* **2005**, 1717–1719.
[11] W. Shi, D. Ge, J. Wang, Z. Jiang, L. Ren, Q. Zhang, *Macromol. Rapid Commun.* **2006**, *27*, 926–930.
[12] L. Pan, H. Qiu, C. Dou, Y. Li, L. Pu, J. Xu, Y. Shi, *Int. J. Mol. Sci.* **2010**, *11*, 2636–2657.
[13] J. Zang, C. M. Li, S. J. Bao, X. Cui, Q. Bao, C. Q. Sun, *Macromolecules* **2008**, *41*, 1053–7057.
[14] C. Debiemme-Chouvy, *Electrochem. Commun.* **2009**, *11*, 298–301.
[15] H. D. Tran, K. Shin, W. G. Hong, J. M. D'Arcy, R. W. Kojima, B. H. Weiller, R. B. Kaner, *Macromol. Rapid Commun.* **2007**, *28*, 2289–2293.
[16] Y. Yang, M. Wan, *J. Mater. Chem.* **2001**, *11*, 2022–2027.
[17] P. M. George, A. W. Lyckman, D. A. LaVan, A. Hegde, Y. Leung, R. Avasare, C. Testa, P. M. Alexander, R. Langer, M. Sur, *Biomaterials* **2005**, *26*, 3511–3519.
[18] H. D. Tran, Y. Wang, J. M. D'Arcy, R. B. Kaner, *ACS Nano* **2008**, *2*, 1841–1848.
[19] A. Wu, H. Kolla, S. K. Manohar, *Macromolecules* **2005**, *38*, 7873–7875.
[20] M. Li, Z. Wei, L. Jiang, *J. Mater. Chem.* **2008**, *18*, 2276–2280.
[21] S. P. Surwade, N. Manohar, S. K. Manohar, *Macromolecules* **2009**, *42*, 1792–1795.
[22] L. Liu, Y. Zhao, N. Jia, Q. Zhou, C. Zhao, M. Yan, Z. Jiang, *Thin Solid Films* **2006**, *503*, 241– 245.
[23] H. D. Tran, D. Li, R. B. Kaner, *Adv. Mater.* **2009**, *21*, 1487–1499.
[24] N. L. Jeon, H. Baskaran, S. K. W. Dertinger, G. M. Whitesides, L. Van De Water, M. Toner, *Nat. Biotechnol.* **2002**, *20*, 826–830.
[25] J. N. L. Albert, T. D. Bogart, R. L. Lewis, K. L. Beers, M. J. Fasolka, J. B. Hutchinson, B. D. Vogt, T. H. Epps, *Nano Lett.* **2011**, *11*, 1351–1357.
[26] C. J. Bettinger, H. A. Becerril, D. H. Kim, B. L. Lee, S. Lee, Z. Bao, *Adv. Mater.* **2011**, *23*, 1257–1261.
[27] N. L. Jeon, S. K. W. Dertinger, D. T. Chiu, I. S. Choi, A. D. Stroock, G. M. Whitesides, *Langmuir* **2000**, *16*, 8311–8316.
[28] T. Sun, L. Feng, X. Gao, L. Jiang, *Acc. Chem. Res.* **2005**, *38*, 644–652.
[29] J. Zang, S. J. Bao, C. M. Li, H. Bian, X. Cui, Q. Bao, C. Q. Sun, J. Guo, K. Lian, *J. Phys. Chem. C* **2008**, *112*, 14843–14847.
[30] L. Xia, Z. Wei, M. Wan, *J. Colloid Interface Sci.* **2010**, *341*, 1–11.
[31] K. Murakoshi, R. Kogure, Y. Wada, S. Yanagida, *Solar Energy Mater. Solar Cells* **1998**, *55*, 113–125.
[32] P. Vukusic, J. R. Sambles, C. R. Lawrence, *Proc. R. Soc. London B* **2004**, *271*, S237–S239.
[33] A. Cassie, S. Baxter. *Trans. Faraday Soc.* **1944**, *40*, 546–551.
[34] R. N. Wenzel, *Ind. Eng. Chem.* **1936**, *28*, 988–994.
[35] A. Cassie, S. Baxter, *Nature* **1945**, *155*, *3923*, 21–22.
[36] X. Feng, L. Jiang, *Adv. Mater.* **2006**, *18*, 3063–3078.
[37] M. Nosonovsky, B. Bhushan, *Adv. Funct. Mater.* **2008**, *18*, 843–855.
[38] W. Barthlott, C. Neinhuis, *Planta* **1997**, *202*, 1–8.
[39] T. Darmanin, M. Nicolas, F. Guittard, *Langmuir* **2008**, *24*, 9739–9746.
[40] K. S. Teh, Y. W. Lu, *IEEE 21st Int. Conf on MEMS* **2008**, 363–366.
[41] A. K. Epstein, B. Pokroy, A. Seminara, J. Aizenberg, *Proc. Natl. Acad. Sci. USA* **2011**, *108*, 995.
[42] P. Kim, A. K. Epstein, M. Khan, L. D. Zarzar, D. J. Lipomi, G. M. Whitesides, J. Aizenberg, *Nano Lett.* **2012**, *12*, 527–533.
[43] P. Kim, W. E. Adorno-Martinez, M. Khan, J. Aizenberg, *Nat. Protocols* **2012**, *7*, 311–327.
[44] T. S. Wong, S. H. Kang, S. K. Y. Tang, E. J. Smythe, B. D. Hatton, A. Grinthal, J. Aizenberg, *Nature* **2011**, *477*, 443–447.
[45] J. Reuber, H. Reinhardt, D. Johannsmann, *Langmuir* **2006**, *22*, 3362–3367.

Received: April 24, 2012
Revised: June 26, 2012
Published online:

DOI: 10.1002/smll.201200888